6

Structure Formation and Glass Transition in Oriented Poly(Ethylene Terephthalate)

Koji Fukao[1], Satoshi Fujii[1], Yasuo Saruyama[1] and Naoki Tsurutani[2]

[1] Department of Polymer Science, Kyoto Institute of Technology, Matsugasaki, Sakyo-ku, Kyoto 606-8585, Japan
fukao@kit.ac.jp
[2] Department of Physics, Kyoto University, Kyoto 606-8502, Japan
turutani@scphys.kyoto-u.ac.jp

Abstract. The ordering process and glass transition of poly(ethylene terephthalate) (PET) in oriented glassy states have been investigated using real time X-ray scattering experiment with synchrotron radiation sources and (temperature modulated) differential scanning calorimetry. The time evolution of the X-ray scattering patterns observed during the isothermal annealing process could well be reproduced using the kinetics of structure formation from the nematic-like structure to the crystal-like structure by way of the smectic structure. During the heating process a corresponding change in X-ray scattering patterns was observed and a continuous structural change from the oriented glassy state to the crystalline state through the smectic-like structure was confirmed. This structural change is accompanied with a continuous increase in the glass transition temperature, which is elucidated using differential scanning calorimetry.

6.1 Introduction

Many recent experiments have shown that a dynamical change occurs prior to the formation of usual crystalline order during crystallization process [1–4]. The dynamical change has been discussed in relation to the structure formation in the early stage of polymer crystallization. Such dynamical change is believed to be essential for understanding the mechanism of polymer crystallization. In our previous work, we investigated the dynamics of the α-process, segmental motion of a polymer chain, especially in the early stage of crystallization of poly(ethylene terephthalate) (PET) using the simultaneous time-resolved measurements of small-angle X-ray scattering (SAXS), wide-angle X-ray scattering (WAXS) and dielectric relaxation spectroscopy (DRS) [3, 4]. In Fig. 6.1, the results obtained with the three different methods are shown for isothermal crystallization at 97.5°C from quenched glassy states. We have found that the dynamics of the α-process changes drastically before the formation of crystalline structure starts. Figure 6.1(a) shows that at isothermal

K. Fukao et al.: *Structure Formation and Glass Transition in Oriented Poly(Ethylene Terephthalate)*, Lect. Notes Phys. **714**, 97–116 (2007)
DOI 10.1007/3-540-47307-6_6

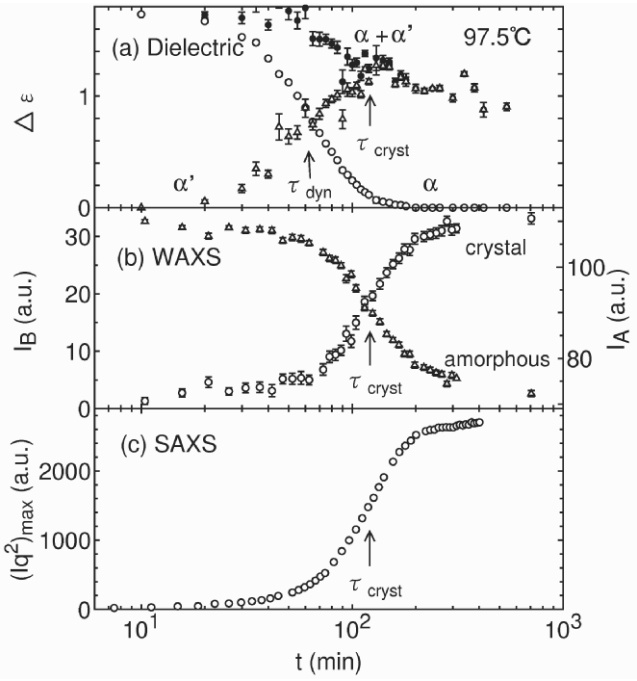

Fig. 6.1. (**a**) Time evolution of the dielectric strength of the α-process ($\circ$) and the α'-process ($\triangle$). The sum of dielectric strengths of the two processes is also plotted with the symbol $\bullet$. (**b**) Time evolution of peak intensity of Bragg reflections $(0\bar{1}1 + 010)$ (I_B, $\circ$) and intensity of amorphous halo (I_A, $\triangle$) (**c**) Time evolution of peak intensity of SAXS profile $Iq^2 vs. q$. All data are obtained during the crystallization process at 97.5°C. The *arrows* indicate the two different characteristic times (τ_{dyn} and τ_{cryst})

process, the strength of the α-process decreases with increasing annealing time, while a new relaxation process (α'-process) appears and its strength increases with time. Figures 6.1(b) and (c) show time evolution of scattering intensities associated with the structure formation over the region of WAXS and SAXS, respectively. Comparing the time scale of structure formation, τ_{cryst}, with that of change in dynamics, τ_{dyn}, we have found that there are two different time scales that are associated with polymer crystallization. This result suggests that the ordering process of polymers cannot be described by only one order parameter, i.e., density, but another order parameter must be required. The candidate of the second order parameter is proposed to be orientational order parameter or conformational order parameter of polymer chains [5].

Oriented PET in the glassy states is a useful system when investigating the effect of orientational order on polymer crystallization mechanism. The crystallization rate of PET is slow enough for time-resolved measurements to

be performed, and PET films can well be uniaxially drawn by cold drawing at room temperature. Recent X-ray measurements on oriented PET have revealed that a smectic structure appears between totally amorphous states, such as melt and glass, and triclinic crystalline states during the isothermal annealing process below the glass transition temperature or the uniaxially drawing process of PET melts [6–12]. The existence of an intermediate structure such as the smectic structure can be regarded as a result coming from the change in orientational order of polymer chains by cold drawing, because the smectic structure cannot be observed during the crystallization process from unoriented amorphous states of PET. A similar smectic ordering induced by shear deformation is observed also in isotactic polypropylene [13].

Our previous work [3,4] showed that there is a drastic change in dynamics of the segmental motion during the crystallization process. From this result we can expect that the glass transition behavior changes during the ordering process from the oriented glassy states. Such information may be very important for understanding the mechanism of the ordering process of these systems. The glass transition in confined geometry such as in crystalline states has been paid much attention in recent years [14].

In this paper, we investigated the ordering process from oriented glassy states of PET during isothermal annealing process on the basis of the measurements on time evolution of scattering intensities of a reflection charactering the smectic structure and also those of a 4-point pattern in the SAXS region. Using a simple kinetic model, we analyze the observed time evolution of the scattering intensities and discuss the kinetics of the formation and decay of the smectic structure during the isothermal annealing process from the oriented glassy states of PET [15]. We also investigated the ordering process during the heating process. For this purpose, we investigated not only X-ray scattering patterns, but also thermal properties of oriented and unoriented glassy states of PET after annealing treatment using differential scanning calorimetry (DSC) and temperature modulated DSC (TMDSC).

6.2 Experiments

Original PET samples are kindly supplied by Toray, Co. Ltd. The as-received PET is unoriented amorphous films with thickness of 0.2 mm. Oriented glassy states of PET are obtained by drawing the original samples at room temperature. The drawing rate and the final draw ratio are controlled to be 4 mm/min and about 4, respectively.

In order to check the degree of chain orientation and overall diffraction pattern of the drawn PET, wide-angle X-ray diffraction photographs were taken for the drawn PET after annealing at 70°C for one hour in an oil bath. For this purpose, we used monochromatic CuK_α X-ray from a conventional rotating anode type of X-ray generator with graphite monochrometer. A vacuum

camera was used in order to improve the signal-to-noise ratio. An imaging plate was also used as a recording media.

For time-resolved X-ray measurements, the oriented glassy states of PET were mounted on the sample holder. The sample holder can be moved quickly from the room temperature side to the higher temperature side which is surrounded by a Cu heater block in a vacuum chamber. After a temperature jump from room temperature to an annealing (crystallization) temperature, change in the X-ray scattering pattern with time was measured during the isothermal annealing process. Annealing temperature was controlled to be a temperature between 63.6°C and 76.3°C. For real-time X-ray measurements during the heating process, the sample was mounted onto a hot-stage (LK-600PM, Linkam). Under N_2 flow, the measurements were done during the heating process at the rate of 10 K/min.

X-ray measurements for $q < 7.5$ nm^{-1} (SAXS and intermediate angle X-ray scattering regions) were performed on RIKEN Beamline I (BL45XU) at SPring8, while those for $q < 30$nm^{-1} (WAXS) were done on BL40B2. Here, q is the scattering vector and is defined as $q = 4\pi \sin\theta/\lambda$, where 2θ is the scattering angle. The wavelength of X-rays, λ, is 0.10 nm and 0.8265 nm for BL45XU and BL40B2, respectively. The detector used in our measurements was a combination of X-ray image intensifier and CCD camera. The camera lengths were 682 mm and 142.5 mm for the measurements on BL45XU and BL40B2, respectively. The obtained scattering data were corrected in order to remove the variation in intensities of incident X-rays and the contribution of background scattering.

For DSC and TMDSC measurements we used commercial instruments DSC10A (Rigaku) and MDSC2920 (TA Instrument), respectively. A segment of the film (∼1.2mg) was cut from the cold-drawn PET film and put into an aluminum pan with an aluminum lid. For the DSC measurements, the heating rate was 20K/min. As an annealing treatment, the sample was heated up to an annealing temperature T_a ($T_a = 65 - 215$°C) at the rate of 20K/min and then cooled down to room temperature at 1K/min. After this annealing process, the DSC measurements were done. For TMDSC measurements, the heating rate was 1 K/min and the period and amplitude of the temperature modulation were 30 sec and 0.5K, respectively.

6.3 Structural Change at Isothermal Annealing Process

6.3.1 X-ray Diffraction Patterns

Wide-angle X-ray diffraction patterns taken on a flat IP are shown in Fig. 6.2 in order to see the overall diffraction pattern of oriented PET. The sample in Fig. 6.2 was annealed at 70°C for one hour. The polymer chains are highly oriented along the draw axis. There are intense broad scattering areas on the equator and sharper streak-like scattering on the meridian. In particular, on

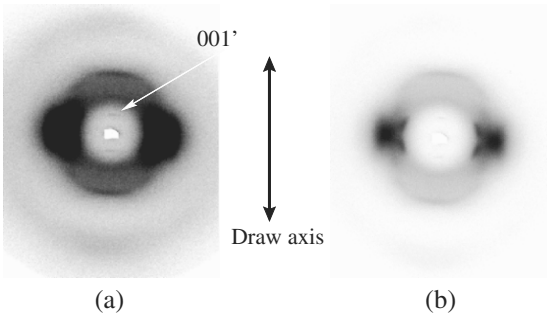

Fig. 6.2. Diffraction patterns in the WAXS region of oriented PET. This sample was annealed at 70°C for one hour. The picture (**a**) is the same as the picture (**b**) except the full scale in intensity. The *arrow* shows the 001' reflection

the meridian there is *a very sharp diffraction spot* near the beam center. We will refer to this reflection as the 001' reflection. The existence of the 001' reflection in the diffraction patterns of the oriented PET was reported by Bonart in 1966 [16]. The lattice spacing corresponding to the 001' reflection was 1.03 nm in the present measurements. In the literature, it is reported that the lattice spacing ranges from 1.02 nm to 1.07 nm depending on the conditions of drawing [6, 8]. The lattice spacing corresponds to the repeating unit of PET monomers along the chain axis. The existence of the 001' reflection on the meridian suggests that PET chains are aligned parallel to each other, and that there is a domain, within which the atomic positions along the chain axis are the same among the neighboring chains. This structure can be regarded as the one similar to the smectic structure of liquid crystals.

As shown in Fig. 6.2(b), we can see four relatively sharp spots just below and just above the equator, in addition to the intense diffuse spots. This suggests that crystalline order is already formed in part at 70°C, below the glass transition temperature of the bulk sample, although the crystalline structure is accompanied by a large degree of disorder.

Figure 6.3 shows time evolution of X-ray scattering patterns of oriented glassy states of PET, observed after the temperature jump from room temperature to 71.2°C using X-ray source from the synchrotron radiation at SPring 8. The draw axis (the z-axis) is shown as an arrow in the figure. The upper row shows the scattering patterns for the q-range of $q < 7.5$ nm^{-1}, and the lower one shows the scattering pattern of the SAXS region of the same scattering patterns as the upper one. The isotropic rings in X-ray scattering patterns are contributions from the scattering from the Kapton films used for the windows of X-ray path. The upper row of figures shows that there is a weak and sharp diffraction spot around $q_z \approx 6.1$ nm^{-1} on the meridian, where q_z is the z-component of the scattering vector. This reflection is the 001' reflection. The

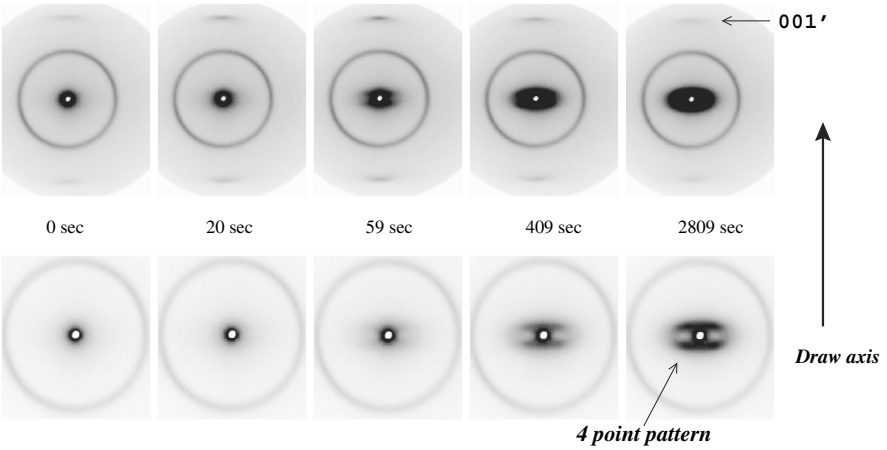

Fig. 6.3. Time evolution of X-ray diffraction patterns of a drawn PET sample annealed at 71.2°C. Diffraction patterns at 0, 20, 59, 409 and 2809 sec are shown. Patterns on the *upper line* are those for $q < 7.5$ nm^{-1}, and those on the *lower line* are for $q < 3.6$ nm^{-1}. The arrow shows the direction of the draw axis (the z-axis).

line width along the direction perpendicular to the meridian can be regarded as a measure of the lateral size of the smectic domain.

The intensity of the reflection 001' increases with time, reaching a maximum at 59sec, and then it begins to decrease gradually with time. The present result shows that the fraction of the smectic structure increases and then decreases with time.

In the lower diffraction pattern in Fig. 6.3, we find that there is almost no SAXS intensity in the beginning of the annealing. However, as time elapses, the intensity increases appreciably in the SAXS region and finally shows a typical 4-point pattern of SAXS. The existence of the 4-point pattern suggests that there is a tilted lamellar structure that is typical of higher order structure of triclinic crystalline PET. In the temperature range around this annealing temperature, 71.2°C, a wide-angle X-ray diffraction measurement revealed that there are very few sharp reflections on the equator, as shown in Fig. 6.2(b). Therefore, the polymer chains in this tilted lamellar structure have a highly disordered (crystalline) structure. Because this highly disordered structure is expected to change into the perfect triclinic structure, we call this structure a *pre-crystalline structure*. According to Asano's model [6], this tilted lamellar structure is formed by tilting PET chains from the draw direction. Here, we can regard the intensity of the 4-point patterns of SAXS as a measure of the fraction of the tilted lamellar structure or the *pre-crystalline* structures.

6.3.2 Integrated Intensity as a Function of Annealing Time

In Fig. 6.4, we show the time evolution of the integrated intensities of the 001' reflection and the 4-point patterns at various annealing temperatures. The integrated intensities of the 001' reflection and the 4-point patterns of SAXS were evaluated from the one-dimensional profile of the scattering intensity at $q_z \approx 6.9$ nm^{-1} and $q_z \approx 0.5$ nm^{-1}, respectively. The contributions from the background and the parasite scattering were subtracted before evaluating the integrated intensities. In Fig. 6.4 it is shown that the intensity of the 001' reflection has a maximum at a time that depends on the annealing temperature. On the other hand, the intensity of the 4-point patterns increases monotonically with time during the isothermal annealing process. From this result, it is found that the fraction of the pre-crystalline structure increases monotonically with time, while the fraction of the smectic structure increases and then decreases with time.

The X-ray diffraction patterns of as-drawn PET samples have a weak 001' reflection on the meridian. This implies that the initial state of oriented PET is a mixture of the nematic structure and the smectic structure, and also that two ordering processes coexist during the isothermal annealing process on PET. (Polymer chains in the nematic structure have a preferred orientation

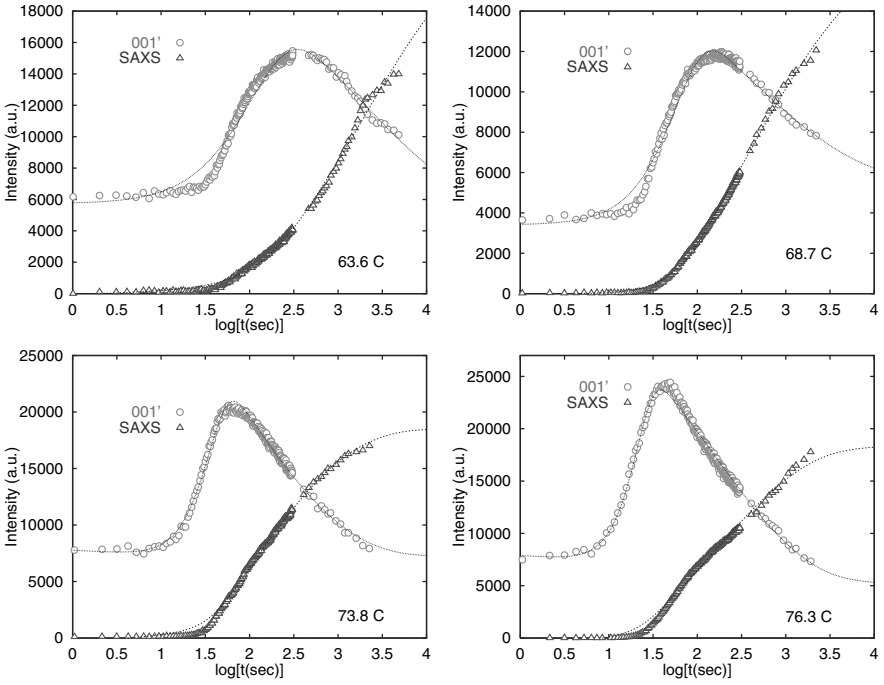

Fig. 6.4. Time evolution of integrated intensity of the 001' reflection (○) and the 4-point patterns of SAXS (△) at various annealing temperatures (63.6°C–76.3°C)

along the draw axis and are randomly aligned along any direction normal to the draw axis.) One is the ordering process from the nematic structure to the smectic structure, and the other is the ordering process from the smectic structure to the pre-crystalline structure. The kinetics of the two ordering processes compete.

It should be noted here that the intensity of the 001' reflection does not seem to decay to zero, but to a finite value, depending on annealing temperature.

6.3.3 Kinetic Model Analysis

Kinetic Model

In order to reproduce the observed time dependence of the intensity of the 001' reflection and the 4-point pattern, we here introduce a kinetic model for the structure formation of PET from the oriented glassy states. In the model, we adopt the following assumptions.

1) The present polymeric system is divided into n_0 equivalent partial regions. There are only three different states for a partial region, that is, *nematic structure*, *smectic structure* and *pre-crystalline structure*. Every partial region takes one of the three states. The number of the nematic regions, smectic regions and pre-crystalline regions at time t are denoted by $n_n(t)$, $n_s(t)$, and $n_t(t)$, respectively.

2) The intensity of the 001' reflection at time t, $I_{001'}(t)$, is proportional to the number of smectic regions at time t, while the integrated intensity of the 4-point pattern in the SAXS regions, $I_{SAXS}(t)$, is proportional to the number of the pre-crystalline regions. Here, the following relations are satisfied:

$$I_{001'}(t) = C \cdot n_s(t) \tag{6.1}$$

$$I_{SAXS}(t) = \tilde{C} \cdot n_t(t) \ , \tag{6.2}$$

where C and $\tilde{C}$ are the constants.

If we assume that the kinetic process from the nematic structure to the smectic structure and from the smectic structure to the pre-crystalline structure are given by the rate constants $\tilde{k}_{ns}$ and $\tilde{k}_{st}$, respectively, the following coupled equations are obtained:

$$\frac{dn_n}{dt} = -\tilde{k}_{ns}(t) n_n \tag{6.3}$$

$$\frac{dn_s}{dt} = \tilde{k}_{ns}(t) n_n - \tilde{k}_{st}(t) n_s \tag{6.4}$$

$$\frac{dn_t}{dt} = \tilde{k}_{st}(t) n_s \ . \tag{6.5}$$

It should be noted that the kinetic process from the nematic structure directly to the pre-crystalline structure without passing the smectic structure is prohibited for simplicity in this model.

Furthermore, it is assumed that the rate constants $\tilde{k}_{ns}$ and $\tilde{k}_{st}$ depend not only on temperature but also on time and are given by the following equations:

$$\tilde{k}_{ns}(t) = k^0_{ns}\alpha t^{\alpha-1} \tag{6.6}$$

$$\tilde{k}_{st}(t) = k^0_{st}\beta t^{\beta-1}\ , \tag{6.7}$$

where k^0_{ns} and k^0_{st} are constants, and α and β are exponents of the power-law with respect to time.

The solution of the above kinetic equations is as follows on condition that $n_n + n_s + n_t \equiv n_0$ (constant):

$$n_n(t) = n^0_n e^{-k^0_{ns}t^\alpha} \tag{6.8}$$

$$\begin{aligned} n_s(t) = &-n^0_n e^{-k^0_{ns}t^\alpha} \\ &+e^{-k^0_{st}t^\beta}\left[\left(1+\beta k^0_{st}\int_0^t s^{\beta-1}e^{-k^0_{ns}s^\alpha+k^0_{st}s^\beta}ds\right)n^0_n + n^0_s\right] \end{aligned} \tag{6.9}$$

$$n_t(t) = n_0 - e^{-k^0_{st}t^\beta}\left[\left(1+\beta k^0_{st}\int_0^t s^{\beta-1}e^{-k^0_{ns}s^\alpha+k^0_{st}s^\beta}ds\right)n^0_n + n^0_s\right]\ , \tag{6.10}$$

where n^0_n and n^0_s are the numbers of the nematic and smectic regions at $t = 0$, respectively.

In case of $k^0_{ns} \to \infty$, there is no difference between nematic structure and the smectic structure. As a result, the kinetic process can be regarded as the process between the two structures (the nematic, or smectic structure, and the pre-crystalline structures), and approximate expressions for $n_n(t)$, $n_s(t)$ and $n_t(t)$ can be obtained from Eqs. (6.8)–(6.10) as follows:

$$n_n(t) \approx 0 \tag{6.11}$$

$$n_s(t) \approx e^{-k^0_{st}t^\beta}(n^0_n + n^0_s) \tag{6.12}$$

$$n_t(t) \approx n_0 - e^{-k^0_{st}t^\beta}(n^0_n + n^0_s)\ . \tag{6.13}$$

The time evolution expressed by Eq. (6.13) is the same as that given by the Avrami equation [17]. This means that the present kinetic model naturally includes the time evolution expressed by the Avrami equation, although the existence of the intermediate state between the initial structure and the final one is taken into account.

In the above procedure, we develop the kinetic model on the assumption that all regions should be in the pre-crystalline structure in the final stage of the kinetic process. However, this assumption is clearly oversimplified. It is more likely that some nematic regions and smectic regions do not transform to any other structures, and that there are still unoriented regions which remain unchanged during the annealing process. Because the existence of the unchanged smectic affects the intensity of the 001' reflection, the contribution of the number of the unchanged smectic regions, n^∞_s, is taken into account by

replacing $n_s(t)$ with $n_s(t)+n_s^{\infty}$ in Eq. (1). Thus, we use the following equation instead of Eq. (1),

$$I_{001'}(t) = C \cdot (n_s(t) + n_s^{\infty}) \; . \tag{6.14}$$

In order to reproduce the observed intensity of the 001' reflection and the 4-point pattern in the SAXS region, we performed a nonlinear least square fit by using Eqs. (2), (6.8)–(6.10), and (14). The solid and dotted curves in Fig. 6.4 were obtained by the above fitting procedure. In Fig. 6.4, it is found that the time evolution of the intensities of both the 001' reflection and the 4-point pattern in the SAXS region can be well reproduced simultaneously by the present kinetic model. In the next sections, we will discuss the several parameters obtained by the fitting.

Characteristic Time

The times characterizing the kinetic processes from the nematic structure to the smectic structure, τ_{ns}, and from the smectic structure to the pre-crystalline structure, τ_{st}, can be defined in the following way:

$$\tau_{ns} = \left(\frac{1}{k_{ns}^0}\right)^{1/\alpha}$$
$$\tau_{st} = \left(\frac{1}{k_{st}^0}\right)^{1/\beta} \; .$$

By using the fitting parameters α, β, k_{ns}^0 and k_{st}^0 at various temperatures, we obtained the temperature dependence of τ_{ns} and τ_{st}, as shown in Fig. 6.5. In this figure, it is found that the functional form of τ_{ns} and τ_{st} with respect to temperature can be expressed by the Arrhenius type of the activation process, although the temperature range investigated here was restricted. According to the Arrhenius law, the characteristic times τ_{ns} and τ_{st} can be given by the following equations:

$$\tau_{ns} = \tau_{ns}^0 \exp\left(\frac{\Delta U_{ns}}{T}\right), \quad \tau_{st} = \tau_{st}^0 \exp\left(\frac{\Delta U_{st}}{T}\right) \; ,$$

where τ_{ns}^0 and τ_{st}^0 are constants, ΔU_{ns} and ΔU_{st} are the activation energy from the nematic structure to the smectic structure and from the smectic structure to the pre-crystalline structure, respectively. From the slope of the straight line in Fig. 6.5, the values of the activation energies can be evaluated as follows:

$$\Delta U_{ns} = (14.0 \pm 2.5) \text{ kcal/mol} \tag{6.15}$$
$$\Delta U_{st} = (21.9 \pm 4.3) \text{ kcal/mol} \tag{6.16}$$

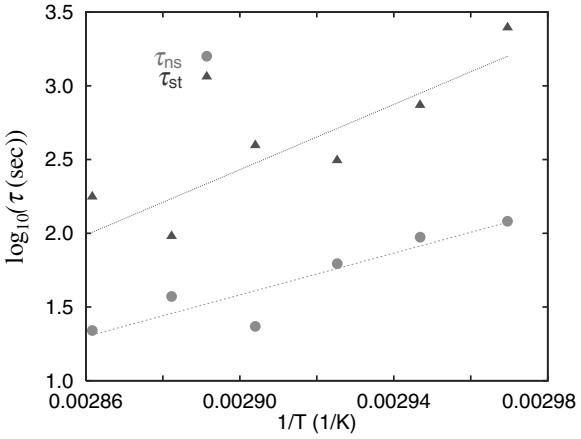

Fig. 6.5. Arrhenius plot of the characteristic times of the transition from nematic structure to smectic structure, τ_{ns}, and the one from smectic structure to pre-crystalline structure, τ_{st}

According to the results by dielectric and mechanical relaxation measurements on PET in [18], we can estimate the averaged activation energy for the α- and β-relaxation processes as follows:

$$\Delta U_\alpha \sim 137 \text{ kcal/mol} , \tag{6.17}$$

$$\Delta U_\beta \sim 15 \text{ kcal/mol} , \tag{6.18}$$

where ΔU_α and ΔU_β are the activation energies for the α- and β-relaxation processes, respectively.

Comparing ΔU_{ns} and ΔU_{st} with ΔU_α and ΔU_β, we find that the values of ΔU_{ns} and ΔU_{st} are much smaller than the activation energy of the α-relaxation process, but they are in relatively good agreement with the activation energy of the β-relaxation process. The structural changes discussed in this paper occur below the glass transition temperature of the bulk sample, and hence it is expected that the α-relaxation process, segmental motion, is prohibited and has no appreciable contribution to the structural change below the glass transition temperature. The observed values of ΔU_{ns} and ΔU_{st} supports this expectation. Furthermore, the β-relaxation process, i.e., the local mode relaxation process, may be a microscopic origin for the structural changes from the nematic structure to the smectic structure and from the smectic structure to the pre-crystalline structure, although the detailed mechanism is still to be elucidated. Real time relaxation measurements during the structural changes are highly desired for this purpose.

Exponent of the Kinetic Equation

The exponents α and β which determine the kinetics of the structural change of oriented PET are shown in Fig. 6.6. The values of α and β are obtained by the fitting procedure mentioned above. In Fig. 6.6, it is found that the exponent α for the kinetics from the nematic structure to the smectic structure decreases from 2.3 to 1 with decreasing temperature within the temperature range investigated here. In the case of the Avrami law [17], the crystalline fraction ϕ_c is given by

$$\phi_c(t) \sim 1 - \exp(-It^d) \ ,$$

where I is the nucleation rate, and d is the exponent. The exponent d is equal to 2 if the mechanism of structural change can be described by a 2-dimensional heterogeneous nucleation and growth. Hence, a possible mechanism for the structural change from the nematic structure to the smectic structure that is consistent with the observed exponent α may be as follows. In a nematic domain, there are smectic regions as heterogeneous nuclei. During the isothermal annealing process, these smectic regions grow two-dimensionally along the direction perpendicular to the chain axis. At a lower temperature, this lateral growth of the smectic domain is hindered, and as a result, the effective dimensionality of the lateral growth is decreased. Analysis of the overall behavior of the diffraction profile along the direction perpendicular to the meridian as a diffuse scattering according to the procedure similar to that shown in Refs. [19, 20] will reveal the nature of the growth of the smectic domain.

As for the structural change from the smectic structure to the pre-crystalline structure, the exponent β is about 0.5 and is almost independent of temperature. The value of the exponent $\beta(\approx 0.5)$ reminds us of the

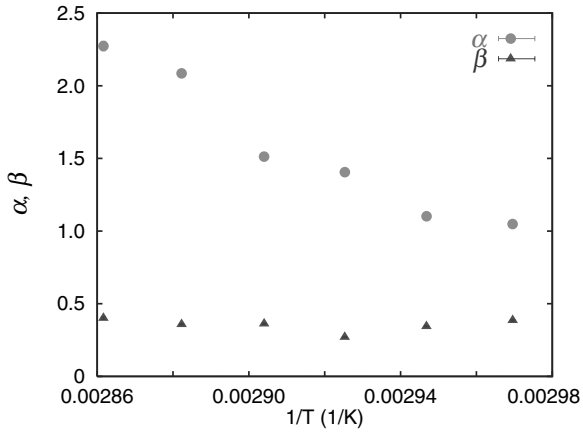

Fig. 6.6. Temperature dependence of the exponent α and β for the transition from the nematic structure to the smectic structure, α, and the one from the smectic structure to the pre-crystalline structure, β

stretched exponential-type of relaxation functions, $\phi(t) = \exp(-(t/\tau)^{\beta_{\mathrm{KWW}}})$ $(0 < \beta_{\mathrm{KWW}} < 1)$ [21]. This function can often be observed in disordered materials and is known as anomalous (slow) relaxation [22]. Hence, this structural formation process is not described by the growth of the pre-crystalline domain, but a slower diffusion process should be taken into account. According to this diffusion picture, it is conjectured that a virtual *particle* diffuses in the real space as a diffusant, and the site through which the particle passes has to change its structure into the pre-crystalline structure if the site belongs to the region of the smectic structure.

6.4 Structural and Thermal Change During the Heating Process

6.4.1 X-ray Scattering Patterns During the Heating Process

In the previous section, the structural change during the isothermal annealing process has been discussed. A similar but larger structural change can be expected during the heating process from room temperature to melting temperature. Figure 6.7 shows the change in the scattering patterns around the position of the 001' reflection on the meridian observed during the heating process from 33°C to 180°C at the rate of 5K/min. At 33°C there is the sharp 001' reflection on the meridian. The intensity of the 001' reflection increases with increasing temperature up to 71°C, and then it begins to decrease. At 100°C the intensities of two off-meridional positions located symmetrically with respect to the meridian are stronger than those around them and two weak spots can be recoginzed. At 180°C the intensities of the spots are enhanced. The two spots correspond to the 001 reflections of the triclinic crystal structure of PET. This result suggests that a continuous structural change from the nematic-like structure to the crystalline structure through the smectic-like structure occurs during the heating process, which is consistent with the results observed during the isothermal annealing process.

We also performed real-time WAXS measurements during the heating process of oriented glassy states of PET, in order to investigate the detailed properties of the continuous structural change. Before WAXS measurements, the samples were annealed at T_a. As an example, in Fig. 6.8, we show the intensity profile along the equator at various temperatures during the heating process at the rate of 10 K/min in the case of T_a=125°C. Figure 6.8(a) shows that the scattering profile does not change below T_a, while Fig. 6.8(b) shows that the intensities of the Bragg reflections such as 010, $\bar{1}10$, and 100 increase with increasing temperature above T_a. From this result, it is found that the ordered structures formed through the annealing procedure before the X-ray scattering measurements are fixed up to the annealing temperature T_a, and a further ordering process occurs only if the temperature proceeds T_a.

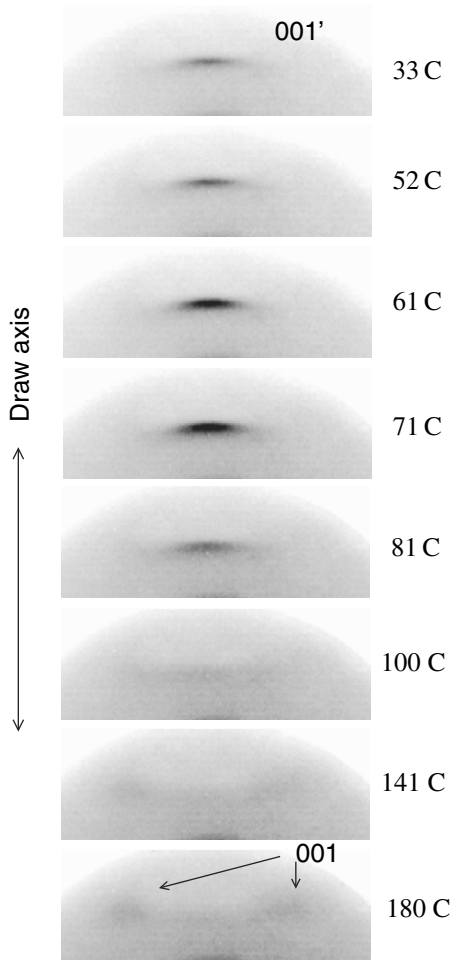

Fig. 6.7. The temperature change in diffraction patterns around the 001' reflection observed during the heating process from 33°C to 180°C at the rate of 5 K/min. The 001' reflection of the smectic structure changes into two 001 reflections of the triclinic crystalline structure of PET with increasing temperature

6.4.2 Thermal Properties of Oriented PET

DSC Measurements

The X-ray scattering measurements revealed that the ordering process in oriented glassy states of PET are generated by a continuous structural change. Here, we will show the corresponding thermal properties observed by DSC. For the DSC measurements, we used the samples of oriented glassy PET that

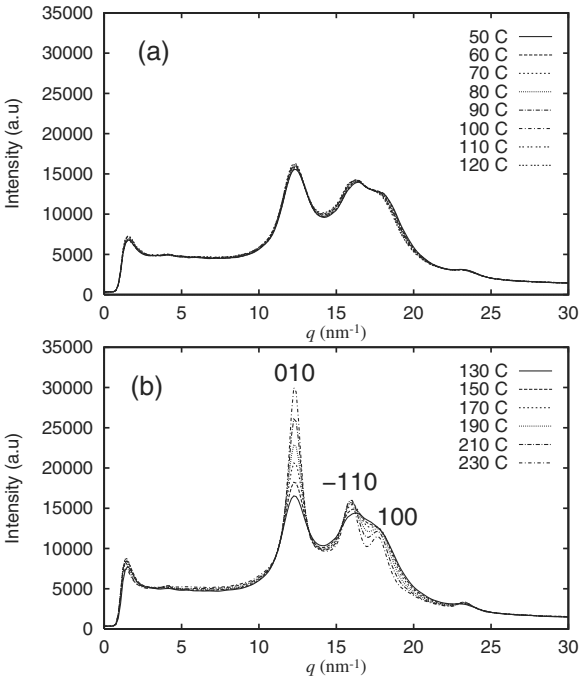

Fig. 6.8. X-ray scattering profile along the equator as a function of the scattering vector at various temperatures during the heating process in oriented glassy states of PET annealed at T_a. Here, $T_a = 125°\mathrm{C}$ and the heating rate is 10K/min. The *upper figure* shows the results for temperatures between 50 and 120°C, and the *lower one* shows those for temperatures above $T_a (\equiv 125°\mathrm{C})$

were drawn at room temperature in the same way as in the X-ray measurements. Figure 6.9 shows DSC thermograms (a) for the unoriented glassy states of PET and (b) for the oriented glassy states of PET without any annealing before measurements. In the case of the unoriented sample, we can observe three typical contributions; the first one is due to the glass transition around 76°C, the second one is due to the crystallization at 145°C, and the third one is due to the melting transition. The exothermic peak temperature for crystallization strongly depends on the heating rate. On the other hand, the DSC thermogram of the oriented sample has two essential differences from that of the unoriented samples. 1) There appears to be no appreciable exothermic signal due to crystallization. 2) There is an anomalous change in the total heat flow at a temperature T_g' just below the glass transition temperature T_g of the unoriented samples. ($T_g = 76°\mathrm{C}$ for unoriented PET and $T_g' = 63°\mathrm{C}$ for non-annealed oriented PET.) A step-like *increase* in the exothermic total heat flow is observed at T_g'. If this change were attributed to the change in heat capacity, the heat capacity would show a step-like *decrease* at T_g'.

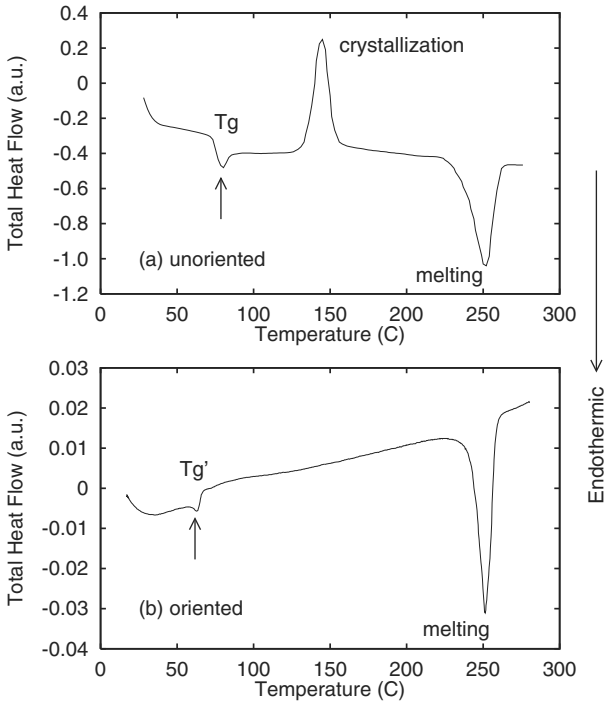

Fig. 6.9. Temperature change in the total heat flow observed during the heating process at 20K/min (**a**) for the unoriented glassy states of PET and (**b**) for the oriented glassy states of PET without any annealing. The negative direction of the total heat flow corresponds to the endothermic heat flow

Figure 6.10 shows DSC thermograms of the oriented PET for various annealing temperatures T_a. The samples were annealed at T_a before the DSC measurements. The measurements were done during the heating process at the rate of 20 K/min. The melting temperature is almost independent of T_a, while the position of the anomaly at T_g' shifts to a higher temperature side with increasing T_a. The value of T_g' is by about 10K larger than the corresponding value of T_a. This result implies that the ordered structure that was formed through the annealing procedure before the DSC measurements is fixed at temperatures below T_a during the heating process. However, if the temperature increases over T_a, the ordering process restarts at $T_g'(> T_a)$ to form a more ordered structure.

As shown in Fig. 6.8, the X-ray scattering patterns show that during the heating process from room temperature, no structural change was observed below T_g', while an ordering process occurs above T_g'. In this sense, some mobility should be activated at T_g' so that the ordering process starts in a similar way as the segmental motions are activated at T_g in the case of the

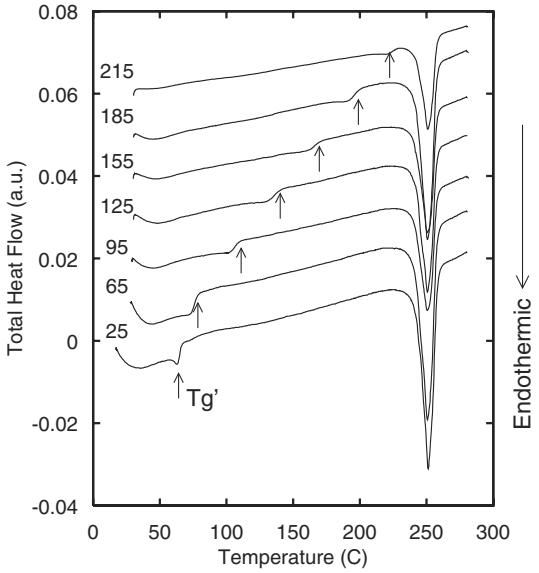

Fig. 6.10. Temperature change in the total heat flow observed during the heating process for the oriented glassy states of PET after annealing at T_a. The *numbers* shown near each curve are annealing temperatures T_a. The *arrows* show the position of the 'glass transition temperature' T_g' for the oriented PET

unoriented PET. Therefore, we can regard the temperature T_g' as the glass transition temperature of the oriented glassy states of PET after the annealing at T_a. However, the observed step-like increase in the exothermic total heat flow at T_g' appears to be totally different from that observed at T_g of the unoriented sample. We try to interpret the observed DSC thermogram around T_g' in the following way: the glass transition occurs at T_g' in the case of the oriented sample and at the same time an ordering process starts. The glass transition induces an endothermic heat flow, while the ordering induces an exothermic heat flow. Hence, both contributions can compete, and as a result the observed DSC thermogram around T_g' can be obtained. As shown in the next section, TMDSC measurements support this interpretation.

Temperature Modulated DSC Measurements

The DSC measurements in the previous section revealed anomalous change in the total heat flow at T_g' where the structural change restarts. We also performed TMDSC measurements in order to investigate the physical origin of the anomalous change at T_g'. In Fig. 6.11, it is found that there is a crossover region where the reversing heat flow changes gradually to a lower value. This region ranges from 80°C to 130°C. The slope of the region above 130°C is

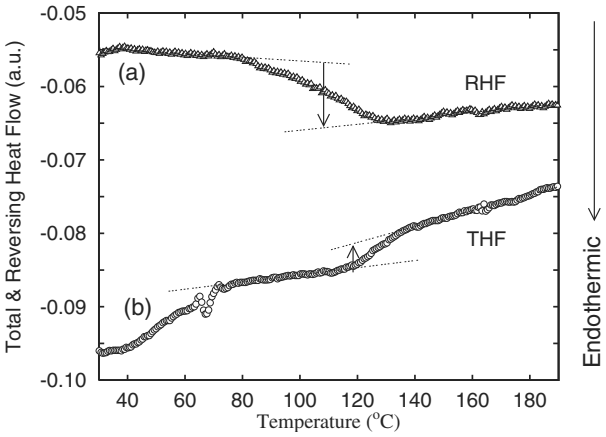

Fig. 6.11. Temperature change in the total and reversing heat flow observed for the oriented PET annealed at T_a=125°C. The curve (a) corresponds to that of the reversing heat flow (RHF) and the curve (b) does to that of the total heat flow (THF).

larger than that below 80°C. Because there should be no contributions from the heat of crystallization, the heat capacity increases in the crossover region and it decreases with increasing temperatures above 130°C. Therefore, we can interpret the temperature dependence of reversing heat flow as follows. The decrease in reversing heat flow between 80°C and 130°C is mainly due to the glass transition because the heat capacity of glassy states is smaller than that of liquid states. On the other hand, the gradual increase in reversing heat flow above 130°C is mainly due to a continuous crystallization that causes the oriented PET to become more ordered structure.

In Fig. 6.11, it is also found that there are two regions where the total heat flow shows anomalous behavior, one is around 70°C and the other is between 110°C and 130°C. The latter one corresponds to the anomalous change in total heat flow observed at T_g' in Fig. 6.10. It can be expected that the observed upper shift of total heat flow at T_g' is mainly due to the heat of crystallization. The position of this anomaly in Fig. 6.11 is different from that in Fig. 6.10. This may be due to the difference in heating rate (20K/min for DSC measurements in Fig. 6.10 and 1K/min for TMDSC measurements in Fig. 6.11.)

Comparing the temperature dependence of the total and reversing heat flow, we can safely regard the temperature T_g' where the total heat flow exhibits an upper shift as the glass transition temperature of the unoriented glassy states of PET. On the other hand, the anomalous change in total heat flow at 70°C in Fig. 6.11, there is no corresponding change in reversing heat flow. This change may be related to some ordering process that has no appreciable contributions to reversing heat flow.

It should be noted that the temperature T_g' where the step-like increase in total heat flow occurs in Fig. 6.10 increases with increasing T_a. This implies that the glass transition temperature of the oriented glassy states of PET increases as the structural order increases during the heating process.

6.5 Concluding Remarks

We investigated the structure formation during the isothermal crystallization (annealing) process from the oriented glassy states of PET using real-time X-ray scattering and thermal measurements. The results obtained are as follows:

1. During the isothermal annealing process at 63.6–76.3°C, the intensity of the 001' reflection from the smectic structure has the maximum at a time, while the intensity of the 4-point pattern in the SAXS region increases monotonically with time.
2. Time dependence of the 001' reflection and the 4-point pattern in the SAXS region can be reproduced by a kinetic model assuming that the fraction of the nematic structure changes into the pre-crystalline structure by way of the smectic structure. A corresponding continuous ordering process could be observed during the heating process.
3. The glass transition temperature of the oriented glassy states increases with increasing degree of ordering.

Although the investigation in this paper mainly concentrated on the time evolution of the 001' reflection and the 4-point pattern in the SAXS region, the measurements of the time dependence of overall diffraction patterns in the WAXS region will be required in order to elucidate the microscopic mechanism of the structure formation in oriented PET. In particular, real-time measurement of the intensity distribution of the meridional reflections of higher order will reveal the detailed mechanism of the structure formation. Real-time relaxation measurements such as dielectric relaxation spectroscopy are also desired for this purpose.

As for the thermal properties, it was revealed that the glass transition temperature of the unoriented glassy states of PET increases extraordinarily with increasing structural order. Recently, it has been reported that there is a rigid amorphous fraction in some polymers [23, 24]. It can be expected that the glass transition temperature of such rigid amorphous fraction is larger than that of usual mobile amorphous fraction, and that it strongly depends on the degree of the ordering.

Acknowledgments

We appreciate A. Koyama, D. Tahara, Y. Miyamoto, Y. Nishikawa, T. Fujisawa, K. Inoue for their helpful collaboration, and Y. Funatsu of Toray

Co., Ltd. for supplying us PET films . The synchrotron radiation experiments were performed at the SPring-8 with the approval of the Japan Synchrotron Radiation Research Institute (JASRI) (Proposal Nos.2001A0306-NDL-np, 2001B0019-NDL-np, 2002A0260-NDL2-np, and 2003B0374-NL2b-np). The work was supported by a Grant-in-Aid for Scientific Research on Priority Areas, Mechanism of Polymer Crystallization (No.12127203) from the Ministry of Education, Culture, Sports, Science and Technology of Japan.

References

[1] M. Imai, K. Mori, T. Mizukami, K. Kaji, T. Kanaya, Polymer **33** (1992) 4451.
[2] C.H. Lee, H. Saito, T. Inoue, Polym. Prep. Jpn. **44** (1995) 735.
[3] K. Fukao and Y. Miyamoto, J. Non-Cryst. Solids, **235-237** (1998) 534.
[4] K. Fukao and Y. Miyamoto, Phys. Rev. Lett., **79** (1997) 4613.
[5] P.D. Olmsted, W.C.K. Poon, T.C.B. McLeish, A.J. Ryan, and N.J. Terrill, Phys. Rev. Lett. **81** (1998) 373.
[6] T. Asano, F.J.B. Calleja, A. Flores, M. Tanigaki, M.F. Mina, C. Sawatari, H. Itagaki, H. Takahashi, I. Hatta, Polymer, **40** (1999) 6475.
[7] D.J. Blundell, A. Mahendrasingam, C. Martin, W. Fuller, D.H. MacKerron, J.L. Harvie, R.J. Oldman, C. Riekel, Polymer, **41** (2000) 7793.
[8] A. Mahendrasingam, D.J. Blundell, C. Martin, W. Fuller, D.H. MacKerron, J.L. Harvie, R.J. Oldman, C. Riekel, Polymer, **41** (2000) 7803.
[9] D.J. Blundell, A. Mahendrasingam, C. Martin, W. Fuller, J. Mat. Sci. **35** (2000) 5057.
[10] G.E. Welsh, D.J. Blundell, A.H. Windle, Macromolecules, **31** (1998) 7562.
[11] G.E. Welsh, D.J. Blundell, A.H. Windle, J. Mat. Sci. **35** (2000) 5225.
[12] D. Kawakami, B.S. Hsiao, S. Ran, C. Burger, B. Fu, I. Sics, B. Chu, T. Kikutani, Polymer **45** (2004) 905.
[13] L. Li and W.H. de Jeu, Faraday Discuss., **128** (2005) 299.
[14] C. Alvarez, I. Sics, A. Nogales, Z. Denchev, S.S. Funari, T.A. Ezquerra, Polymer **45** (2004) 3953.
[15] K. Fukao, A. Koyama, D. Tahara, Y. Kozono, Y. Miyamoto, N. Tsurutani, J. Macromol. Sci. Part.B-Phys. **B42** (2003) 717.
[16] R. Bonart, Kolloid-Z, **213** (1966) 1.
[17] M. Avrami, J. Chem. Phys. **7** (1939) 1103, **8** (1940) 212, **9** (1941) 177.
[18] N.G. McCrum, B.E. Read, and G. Williams, 'Anelastic and Dielectric Effects in Polymeric Solids', (John Wiley and Sons Ltd, London, 1967), p. 506–507, Fig. 13.3.
[19] K. Fukao, J. Chem. Phys. **101** (1994) 7882.
[20] K. Fukao, J. Chem. Phys. **101** (1994) 7893.
[21] G. Williams, D.C. Watts, Trans. Faraday Soc. **66** (1970) 80.
[22] M.F. Shlesinger, E.W. Montroll, Proc. Natl. Acad. Sci. USA **81** (1984) 1280.
[23] H. Xu, B.S. Ince, P. Cebe, J. Polym. Sci. Part B: Polym. Phys. **41** (2003) 3026.
[24] B. Natesan, H. Xu, B.S. Ince, P. Cebe, J. Polym. Sci. Part B: Polym. Phys. **42** (2004) 777.